Letter

Microwave power harvesting using resonator-coupled double quantum dot photodiode

Subhomoy Haldar,[1,*] Drilon Zenelaj,[2] Patrick P. Potts,[3] Harald Havir,[1] Sebastian Lehmann,[1] Kimberly A. Dick,[1,4] Peter Samuelsson,[2] and Ville F. Maisi[1,†]

[1]*NanoLund and Solid State Physics, Lund University, Box 118, 22100 Lund, Sweden*

[2]*NanoLund and Mathematical Physics, Lund University, Box 118, 22100 Lund, Sweden*

[3]*Department of Physics, University of Basel, Klingelbergstrasse 82, 4056 Basel, Switzerland*

[4]*Center for Analysis and Synthesis, Lund University, Box 124, 22100 Lund, Sweden*

(Received 27 June 2023; revised 8 January 2024; accepted 29 January 2024; published 15 February 2024)

We demonstrate a microwave power-to-electrical energy conversion in a resonator-coupled double quantum dot. The system, operated as a photodiode, converts individual microwave photons to electrons tunneling through the double dot, resulting in an electrical current flowing against the applied voltage bias at input powers down to 1 fW. The device attains a maximum power harvesting efficiency of 2%, with the photon-to-electron conversion efficiency reaching 12% in the single-photon absorption regime. We find that the power conversion depends on thermal effects showing that thermodynamics plays a crucial role in the single-photon energy conversion.

DOI: 10.1103/PhysRevB.109.L081403

Nanoscale energy conversion, enabled by the revolutionary advancements in science and technology [1,2], is key to the functionality of solar cells [3,4], telecommunication systems [5], and nanoscale sensing [6]. Precise control and manipulation of energy at the nanoscale are of fundamental importance to quantum thermodynamics [7], circuit quantum electrodynamics [8,9], and quantum information processing [10]. For these purposes, quantum dots (QDs) have emerged as compelling candidates, offering a quantum channel to control the energy and information flow [9,11–15]. As demonstrated by previous experiments and theory, QDs have a large potential for thermoelectric power harvesting/heat engines [16–18], information-to-work conversion [14,19], and for the conversion of infrared radiation into usable electric power [20,21].

Recently, the investigation of microwave photons interacting with QDs has garnered considerable interest, leading to the development of microwave detectors [22–25], microwave microscopy [26], and lasing operation in the microwave regime [27–29]. These advances provide a unique platform to explore the physics of condensed matter systems and astronomy with an energy resolution of a few tens of μeV [30–32]. Of particular interest is the harvesting of microwave power, extensively investigated for large powers (> μW) [5,33,34] where a classical wave description of the radiation is appropriate. However, to date experimental demonstrations of microwave power harvesting in the low-power quantum regime, characterized by single-photon absorption, are lacking, leaving possibilities for utilizing microwave energy at the most fundamental level unexplored.

Here, we present an experimental realization of a microwave power harvester capable of operating in the single-photon absorption regime. An electron occupying a double quantum dot (DQD) embedded in a superconducting resonator absorbs a microwave photon and undergoes photon-assisted tunneling, generating an electrical current from a source (S) to a drain (D) lead. This scheme has previously been demonstrated for microwave photodetectors in Refs. [23,24], where S and D are kept at equal chemical potential and the energy gained by the tunneling electrons is dissipated in the leads. In this Letter, by instead operating the photodetector against an applied bias, part of the energy gained by absorbing a microwave photon is converted into electrical energy. We hence realize microwave power harvesting in the quantum regime, observing a maximal power harvesting efficiency of 2% at 1 fW input power. Our results open up for applications in the single-photon absorption regime, in on-chip power delivery in quantum circuits [9,10] and astronomy, enabling energy collection from cosmic electromagnetic radiation [30,32,35].

The device operation is illustrated schematically in Fig. 1(a). In the single-photon absorption regime, under ideal operation conditions [24] every single photon is converted into an electron tunneling through the DQD (red arrows), against the bias. At low temperatures, for a bias approaching the photon energy, the efficiency of the power conversion as well as the photon-to-electron conversion, or photodetection, efficiency thus reach unity. For an increasing temperature, thermally induced excitations in the DQD block the photon-assisted tunneling and lead to a backflow of electrons (blue arrows), reducing both the photodetection and power conversion efficiencies. We here present a theoretical estimate of the thermodynamic maximum of the power

*subhomoy.haldar@ftf.lth.se
†ville.maisi@ftf.lth.se

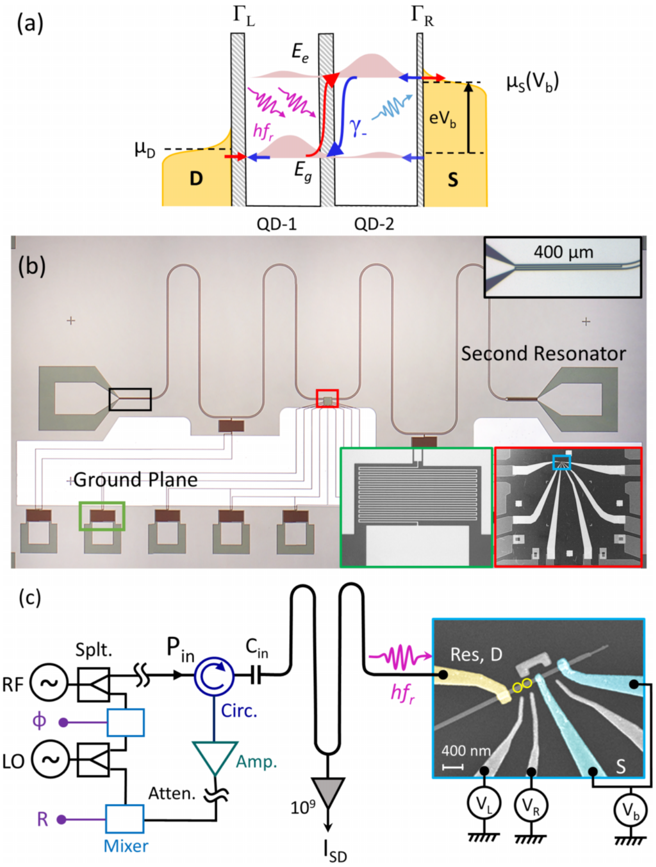

FIG. 1. (a) Schematic of device energy band diagram. Red arrows show an electron absorbing a photon of energy hf_r and tunneling through the DQD against a bias voltage V_b. Blue arrows show tunneling processes in the direction of applied bias. (b) Optical micrograph of the hybrid device. Insets depict the input coupler of the resonator, inductive filtering on the dc lines, and the central part of the device showing the connections to the DQD. (c) False-colored scanning electron micrograph showing the nanowire device with the schematic layout of the rf and transport measurement scheme. Bias is applied on the blue leads across the DQD (indicated by yellow circles) and current I_{SD} is measured via the middle point of the resonator that directly connects the DQD (yellow lead).

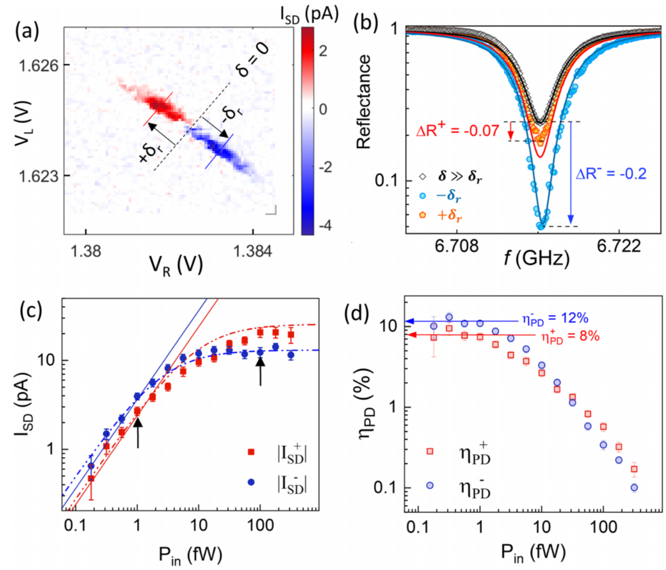

FIG. 2. (a) Measured photocurrent I_{SD} as a function of gate voltages V_L and V_R with $V_b = 0$ and microwave drive $P_{in} = 1$ fW. The black dashed line indicates the $\delta = 0$ detuning line. (b) Microwave reflection coefficient as a function of drive frequency measured in the Coulomb blockade regime (at $\delta \gg \delta_r$) and photodetection point (at $\delta = \pm\,\delta_r$) with $P_{in} = 1$ fW. (c) Photocurrent and (d) photon-to-electron conversion efficiency as a function of P_{in}. Solid (dashed) lines show the theoretically fitted curves at the low (large) drive regime.

conversion efficiency. Moreover, increasing the power beyond the single-photon absorption regime reduces the photodetection and power conversion efficiencies as well. Our scheme is qualitatively different from conventional microwave power conversion with rectifier antennas, or rectennas [36–39]. Rectennas work at high powers, where the radiation can be described as classical waves. The maximum power conversion efficiency, which can approach unity, is set by the device properties and not temperature—operation is typically at ambient temperatures.

The device comprises a semiconductor DQD dipole coupled to a one-port waveguide resonator [Fig. 1(b)]. The DQD is formed by three segments of wurtzite barriers that confine electrons in two zinc-blende islands in an InAs nanowire [40–42]. Two plunger gate voltages V_L and V_R control the electrochemical potential of QD-1 and QD-2, respectively. The D lead of the DQD directly connects to the resonator which has a fundamental resonance at $f_r = 6.715$ GHz. The current I_{SD} across the DQD is measured via the resonator voltage node point. The nanowire also hosts a third (sensor) dot coupled to a readout resonator with fundamental resonance at 6.31 GHz ($\neq f_r$) [see Fig. 1(b)]. We do not use the sensor dot or the second resonator in the present study. To avoid any influence from the third dot, we apply the same bias V_b to both sides of the sensor dot [Fig. 1(c)]. Measurements are performed in a dilution refrigerator with an electronic temperature of $T_e \approx 60$ mK. The Supplemental Material (SM) [43] presents the dc current-bias measurements of the DQD and details of the rf heterodyne circuit used in this work. The same device has been used in Ref. [44] to investigate wave-particle interplay by studying the energetics of the microwaves during the photodiode operation. For the power conversion, we drive the system with the cavity resonance frequency f_r, and only use $f \neq f_r$ for the device characterization.

We start by measuring the photoresponse without applying a bias voltage. Figure 2(a) shows the photocurrent as a function of gate voltages with microwave power $P_{in} = 1$ fW. By varying V_L and V_R, we move the energy levels of the respective dots and thus change the detuning δ. In Fig. 2(a), we observe that $I^{\pm}_{SD}$ in the direction of $\pm\delta$ reaches a maximum when the energy gap between the hybridized states of the DQD matches the photon energy, $hf_r = E_e - E_g = \sqrt{\delta_r^2 + 4t^2}$, where E_g (E_e) denotes the energy of the ground (excited) state and t denotes the interdot tunnel coupling [12,24]. Due to the energy transfer from the photons to the electrons, the DQD at $\pm\delta_r$ introduces an additional loss channel ($\kappa^{\pm}_{DQD}$) to the resonator photon mode. Figure 2(b) presents the changes to the resonator response in the different detuning conditions due to this additional loss channel. We then vary $P_{\rm in}$ and plot the measured $I_{\rm SD}$ at $\pm\delta_r$ in Fig. 2(c). The corresponding photon-to-electron conversion efficiency, $\eta_{\rm PD} = I_{\rm SD} hf_r/eP_{\rm in}$, is plotted in Fig. 2(d), which shows a plateau in the low-power regime with $\eta^-_{\rm PD}$ reaching 12%. Note that $\eta_{\rm PD}$ encompasses the entire process of photon-assisted tunneling, and thus corresponds to the external quantum efficiency (see SM [43]).

Next, to explore the ability of our device as a microwave power harvester, we consider $P_{\rm in} = 1$ and 100 fW. This represents two distinct physical regimes, with linear and nonlinear responses to the photon flux [see the marked arrows in Fig. 2(c)]. Figures 3(a) and 3(b) present the maximum $I^\pm_{\rm SD}$ in the plunger gate space recorded as a function of V_b. The corresponding electrical power out $P_{\rm out} = I_{\rm SD}V_b$ is shown in Figs. 3(c) and 3(d). For a wide range of bias voltages, $I_{\rm SD}$ flows against V_b and hence, microwave energy is converted into electrical energy. The shaded areas indicate the overall bias range where power harvesting takes place. For opposite detuning, V_b drives the electronic transport in the bias direction, resulting in a sharp increase in the power dissipation. The blue (black) arrow of Fig. 3(c) depicts the amount of power harvested (dissipated) with $V_b = 5\,\mu$V when the energy levels are detuned to $-\delta_r$ $(+\delta_r)$.

We employ the commonly used [36,37] definition of the power harvesting efficiency as the ratio of the dc electric output power to the ac input power from the microwave drive, as

$$\eta_E = \frac{P_{\rm out}}{P_{\rm in}} = \frac{I_{\rm SD}V_b}{P_{\rm in}}. \tag{1}$$

Figures 3(e) and 3(f) plot η_E as a function of V_b for the two input powers. For $eV_b \ll hf_r$, the η_E increases linearly with V_b. In this low-bias regime, the bias-independent nature of $\eta_{\rm PD}$ allows us to observe a linear dependence of $\eta^\pm_{\rm E} = \eta^\pm_{\rm PD}eV_b/hf_r$, as illustrated by the dashed purple lines in Figs. 3(e) and 3(f). Further increasing V_b causes a sublinear response in η_E, which then reaches a maximum $\eta_E^{\rm max}$ with V_b^m, followed by a sharp decrease when eV_b approaches the photon energy hf_r. For $P_{\rm in} = 1$ fW, the device attains the maximum power harvesting efficiency $\eta_E^{-\rm max} = 2\%$ with positive bias $V_b^m = 10\,\mu$V as marked by (A) in Fig. 3(e).

The energy of the absorbed radiation contributing to the power harvesting is set by the DQD level detuning δ. For the low-power case, with $P_{\rm in} = 1$ fW, it is clear from Fig. 3(g) [see also Fig. 2(a)] that power is harvested at the level detuning $\delta \approx hf_r$. For $\delta \gg hf_r$ the photocurrent and hence the power harvesting becomes vanishingly small. This shows that the power harvesting occurs in the single-photon absorption regime, with negligible contributions from multiple-photon absorption. In line with this observation, the power harvesting efficiency in Fig. 3(e) vanishes when the applied bias eV_b exceeds the single-photon energy hf_r. On the contrary, for $P_{\rm in} = 100$ fW, power harvesting occurs even when $eV_b > hf_r$, as seen in Fig. 3(f). This can mainly be attributed to the nonlinear, multiple-photon absorption process. Moreover, the broadening of the photocurrent spot around δ_r with strong drive also enables power harvesting at $eV_b > hf_r$.

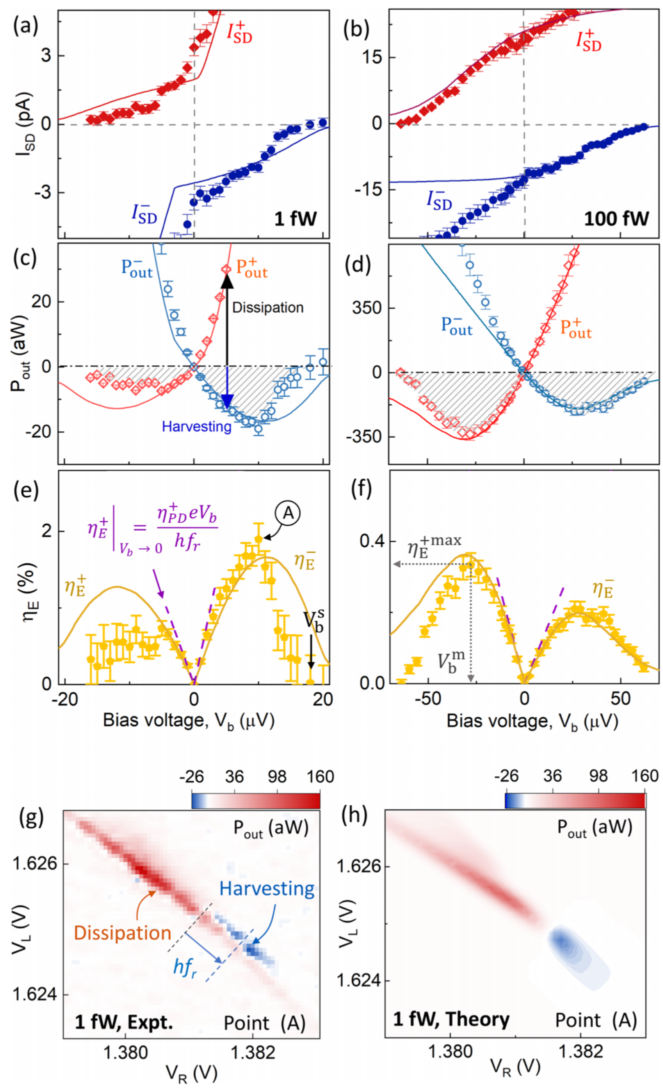

FIG. 3. Photocurrent measured with an applied bias V_b across the DQD for (a) 1 fW and (b) 100 fW input microwave powers. The solid lines depict the numerically calculated results for the two detuning configurations. (c) and (d) show the corresponding power harvested or dissipated by the device, while (e) and (f) show the corresponding power harvesting efficiency η_E for the two input powers. The bias setting required to achieve maximum η_E of 2% is marked with point (A) in (e). (g) and (h) present experimental and theoretical results comparing the power harvested and dissipated in the plunger gate space with $P_{\rm in} = 1$ fW and $V_b = 10\,\mu$V, which corresponds to point (A) in (e).

The effect of temperature on the power conversion efficiency is of particular interest in our device, where the thermal energy (k_BT_e) of the electrons cannot be neglected compared to the photon energy hf_r. For an applied bias voltage such that the chemical potentials of the drain and source leads approach the energy levels (E_g, E_e) of the DQD, thermal fluctuations in the electron population near the Fermi levels of the reservoirs induce excitations to the DQD occupancy. As shown in Fig. 1(a), this hinders the photon absorption in the DQD (red arrows) and also leads to a backflow of the electrons (blue arrows), suppressing the power conversion efficiency. To obtain a qualitative understanding of these thermodynamic effects on the power harvesting, we consider a basic, mean-field master equation model (see SM for details [43]), assuming low drive power, symmetric tunnel couplings, no interdot relaxation, and no internal losses in the resonator. At $T_e = 0$, these assumptions give $\eta_E = 1$ as well as $\eta_{\rm PD} = 1$. At nonzero temperatures, $k_B T_e \ll hf_r$, the power conversion efficiency in Eq. (1), maximized over bias voltage, can then conveniently be written

$$\eta_E^{\rm max} = \frac{eV_b^m}{hf_r}\eta_{\rm PD}^{\rm max}, \tag{2}$$

where $V_b^m = hf_r - 2k_B T_e \ln(1/2\sqrt{hf_r/k_B T_e} + 9/4)$ is the maximizing bias voltage and $\eta_{\rm PD}^{\rm max} = (1 - k_B T_e/hf_r)$ is the photodetection efficiency attainable at V_b^m. Equation (2) shows that two separate thermal effects suppress the maximum power harvesting efficiency $\eta_E^{\rm max}$. First, the photodetection efficiency $\eta_{\rm PD}$ is suppressed by increasing temperature. Second, the maximizing bias voltage V_b^m decreases to a value below the photon energy hf_r. As a result, we have $\eta_E^{\rm max} \leqslant \eta_{\rm PD}^{\rm max}$. Moreover, since $\eta_{\rm PD}^{\rm max}$ is the photodetection efficiency at V_b^m and not at zero bias (for which it is maximal), it is clear that temperature effects have a more detrimental influence on $\eta_E^{\rm max}$ than on the maximal $\eta_{\rm PD}$. This is in agreement with our findings that $\eta_{\rm E}^{\rm max} = 2\%$ while the maximal, low-power, low-bias $\eta_{\rm PD}$ reaches 12%.

The device properties are obtained by comparing the zero applied bias photocurrent data of Fig. 2(c) and the resonator response in Fig. 2(b) with theoretical predictions. We use the quantum master equation approach of Khan *et al.* [24] with the additional features of $I_{\rm SD}^+ \neq I_{\rm SD}^-$ which allow us to determine the tunnel rates at the left ($\Gamma_{\rm L}$) and right ($\Gamma_{\rm R}$) QD-lead barriers individually. We calculate six unknown parameters: tunnel rates $\Gamma_{\rm L}, \Gamma_{\rm R}$, interdot tunnel coupling t, charge dephasing rate γ_ϕ, interdot relaxation rate γ_-, and cavity-DQD coupling constant g, by fitting the following six features: two photocurrent slopes in the low-power limit of Fig. 2(c), two photocurrent plateaus in the high-power limit of Fig. 2(c), and the rf reflectance curves measured at $\pm\delta_r$ in Fig. 2(b). We note that t contributes to the hybridization of the DQD levels and that the coupling constant g sets the interaction strength between the resonator and DQD, determining the response of the DQD to the drive of the microwave cavity [23,24,31]. The solid (dashed) lines in Fig. 2(c) show the fitted curves in the linear (nonlinear) response regime using Eqs. (S6) and (S9) (see SM for further details [43]). We see that the theoretical results capture the essential features of the experimental data, with the best fitting yielding $\Gamma_{\rm L}/2\pi = 27\,{\rm MHz}$, $\Gamma_{\rm R}/2\pi = 5400\,{\rm MHz}$, $\gamma_-/2\pi = 36\,{\rm MHz}$, tunnel coupling $t = 2.5\,\mu{\rm eV}$, $\gamma_\phi/2\pi = 1500\,{\rm MHz}$, and $g/2\pi = 27\,{\rm MHz}$. Importantly, we find $\Gamma_{\rm R} \gg \Gamma_{\rm L}, \gamma_-$, which is causing the asymmetry in the device operation. The fits [Eq. (S14)] to the reflectance spectra in Fig. 2(b) provide the couplings, $\kappa_{\rm DQD}^+/2\pi = 4g^2/2\pi\tilde{\Gamma}^+ = 0.4\,{\rm MHz}$ and $\kappa_{\rm DQD}^-/2\pi = 4g^2/2\pi\tilde{\Gamma}^+ = 1.0\,{\rm MHz}$, where $\tilde{\Gamma}^+$ ($\tilde{\Gamma}^-$) is the total decoherence rate at $+\delta_r$ ($-\delta_r$). Based on the scatter of the data points and their correspondence to the fits, we estimate an uncertainty of approximately 10% for all the parameter values.

To get further insight into the asymmetry of the device operation, we derive an expression for the photocurrent in zero-bias setting for low drive power and $\Gamma_{0e} \gg \kappa$, reading

$$I_{\rm SD}/e = \frac{P_{\rm in}}{hf_r}\frac{\kappa_{\rm c}}{\kappa}\frac{4\kappa_{\rm DQD}\kappa}{(\kappa_{\rm DQD}+\kappa)^2}\frac{\Gamma_{0e}}{(\Gamma_{0e}+\gamma_-)}p_f, \tag{3}$$

where $\Gamma_{g0} = \Gamma_{g{\rm L}} + \Gamma_{g{\rm R}}$ ($\Gamma_{0e} = \Gamma_{{\rm L}e} + \Gamma_{{\rm R}e}$) is the total tunnel rate into the ground (out of the excited) state and $p_f = (\Gamma_{g{\rm L}}\Gamma_{{\rm R}e} - \Gamma_{g{\rm R}}\Gamma_{{\rm L}e})/\Gamma_{0e}\Gamma_{g0}$ denotes the directivity of the DQD. Here, $\Gamma_{({\rm L/R})(g/e)}$ ($\Gamma_{(g/e)({\rm L/R})}$) denotes the tunneling rates out from (into) the DQD ground/excited state from the left/right leads. These tunnel rates are the couplings $\Gamma_{\rm L/R}$ weighted with the corresponding hybridization of the DQD state. The asymmetry of the photoresponse can be traced back to the asymmetry in $\kappa_{\rm DQD}$. At $+\delta_r$, the tunnel rate out of the excited state is much larger than at $-\delta_r$ due to $\Gamma_{\rm R} \gg \Gamma_{\rm L}$. This results in a larger decoherence rate $\tilde{\Gamma}$ at $+\delta_r$, which reduces the effective coupling $\kappa_{\rm DQD}$ in analogy to the Zeno effect [45]. In addition, the fourth term in Eq. (3) adds a smaller contribution to the asymmetry.

In the high-power regime [Eq. (S9)], the ground and excited states become equally populated, and thus the dynamics within the DQD can be neglected. Here, the saturation photocurrent only depends on the in- and out-tunneling rates and is given by $I_{\rm SD}^*/e = p_f/(1/\Gamma_{g0} + 2/\Gamma_{0e})$, where the factor of 2 arises from the fact that the DQD spends only half of the time in the excited state. In the limit of large asymmetry $\Gamma_{\rm L} \ll \Gamma_{\rm R}$, the smallest rate among Γ_{g0} and Γ_{0e} determines the $I_{\rm SD}^*$ and the ratio of currents becomes $I_{\rm SD}^{*+}/I_{\rm SD}^{*-} = 2\Gamma_{{\rm L}e}^+/\Gamma_{g{\rm L}}^- = 2$, which is in good agreement with our experiment $I_{\rm SD}^{*+}/I_{\rm SD}^{*-} = 1.7$.

Based on the parameter values extracted from the zero-bias data, we can numerically evaluate the finite-bias current $I_{\rm SD}^\pm$ and the corresponding power conversion at $T_e = 60$ mK. The solid lines in Figs. 3(a)–3(f) depict the results. Furthermore, in Figs. 3(g) and 3(h), we compare the experiment and theory results showing the amount of power harvested and dissipated by the device in the plunger gate space corresponding to the point (A) of Fig. 3(e). Once again, the theoretical curves are found to be in good agreement with the experimental data and reproduce the asymmetric η_E in the two detuning configurations. We however note that for chemical potentials close to the DQD energies our master equation approach formally breaks down, which may explain the discrepancy between experiment and theory at $|V_b| \sim hf_r$ in Figs. 3(c) and 3(e). Moreover, despite our theoretical approach not accounting for multiphoton processes, the agreement between experiment and theory for $P_{\rm in} = 100$ fW in Fig. 3(c) and 3(e) is still good (see SM for further discussion [43]).

In conclusion, we have demonstrated a microwave resonator-DQD power harvester operating in the femtowatt-power, single-photon absorption regime where a quantum description of the incoming radiation is appropriate and conventional rectenna power harvesters do not work. We achieve a maximum power conversion efficiency of 2% and a photon-to-electron conversion efficiency reaching 12%. Our controllable and versatile microwave power harvester opens up avenues of experiments enabling energy collection at the single-photon absorption limit, to explore the fundamental aspects of quantum thermodynamics, quantum optics, and astrophysics.

We acknowledge fruitful discussions with Antti Ranni, Claes Thelander, Adam Burke, Martin Leijnse, and Andreas Wacker, and financial support from the Knut and Alice Wallenberg Foundation through the Wallenberg Center for Quantum Technology (WACQT), the Foundational Questions Institute, a donor advised fund of Silicon Valley Community Foundation (Grant No. FQXi-IAF19-07), NanoLund, and Swedish Research Council (Dnr 2019-04111). We also thank Jonas Bylander, Simone Gasparinetti, and Anita Fadavi Roudsari from the Chalmers University of Technology for fruitful discussions to improve the superconducting cavity. P.P.P. acknowledges funding from the Swiss National Science Foundation (Eccellenza Professorial Fellowship No. PCEFP2_194268).

[1] F. P. G. de Arquer, D. V. Talapin, V. I. Klimov, Y. Arakawa, M. Bayer, and E. H. Sargent, Semiconductor quantum dots: Technological progress and future challenges, Science **373**, eaaz8541 (2021).

[2] M. Zhang, W. Cai, Z. Wang, S. Fang, R. Zhang, H. Lu, A. E. Aliev, A. A. Zakhidov, C. Huynh, E. Gao *et al.*, Mechanical energy harvesters with tensile efficiency of 17.4% and torsional efficiency of 22.4% based on homochirally plied carbon nanotube yarns, Nat. Energy **8**, 203 (2023).

[3] P. Krogstrup, H. I. Jørgensen, M. Heiss, O. Demichel, J. V. Holm, M. Aagesen, J. Nygard, and A. Fontcuberta i Morral, Single-nanowire solar cells beyond the Shockley–Queisser limit, Nat. Photon. **7**, 306 (2013).

[4] O. E. Semonin, J. M. Luther, S. Choi, H.-Y. Chen, J. Gao, A. J. Nozik, and M. C. Beard, Peak external photocurrent quantum efficiency exceeding 100% via MEG in a quantum dot solar cell, Science **334**, 1530 (2011).

[5] L. Portilla, K. Loganathan, H. Faber, A. Eid, J. G. D. Hester, M. M. Tentzeris, M. Fattori, E. Cantatore, C. Jiang, A. Nathan *et al.*, Wirelessly powered large-area electronics for the internet of things, Nat. Electron. **6**, 10 (2023).

[6] Z. L. Wang, Self-powered nanosensors and nanosystems, Adv. Mater. **24**, 280 (2012).

[7] J. P. Pekola, Towards quantum thermodynamics in electronic circuits, Nat. Phys. **11**, 118 (2015).

[8] R. Kokkoniemi, J.-P. Girard, D. Hazra, A. Laitinen, J. Govenius, R. Lake, I. Sallinen, V. Vesterinen, M. Partanen, J. Tan *et al.*, Bolometer operating at the threshold for circuit quantum electrodynamics, Nature (London) **586**, 47 (2020).

[9] A. A. Clerk, K. W. Lehnert, P. Bertet, J. R. Petta, and Y. Nakamura, Hybrid quantum systems with circuit quantum electrodynamics, Nat. Phys. **16**, 257 (2020).

[10] A. Auffèves, Quantum technologies need a quantum energy initiative, PRX Quantum **3**, 020101 (2022).

[11] L. Childress, A. S. Sørensen, and M. D. Lukin, Mesoscopic cavity quantum electrodynamics with quantum dots, Phys. Rev. A **69**, 042302 (2004).

[12] W. G. van der Wiel, S. De Franceschi, J. M. Elzerman, T. Fujisawa, S. Tarucha, and L. P. Kouwenhoven, Electron transport through double quantum dots, Rev. Mod. Phys. **75**, 1 (2002).

[13] A. Chatterjee, P. Stevenson, S. De Franceschi, A. Morello, N. P. de Leon, and F. Kuemmeth, Semiconductor qubits in practice, Nat. Rev. Phys. **3**, 157 (2021).

[14] D. Barker, M. Scandi, S. Lehmann, C. Thelander, K. A. Dick, M. Perarnau-Llobet, and V. F. Maisi, Experimental verification of the work fluctuation-dissipation relation for information-to-work conversion, Phys. Rev. Lett. **128**, 040602 (2022).

[15] R. Wang, R. S. Deacon, J. Sun, J. Yao, C. M. Lieber, and K. Ishibashi, Gate tunable hole charge qubit formed in a Ge/Si nanowire double quantum dot coupled to microwave photons, Nano Lett. **19**, 1052 (2019).

[16] M. Josefsson, A. Svilans, A. M. Burke, E. A. Hoffmann, S. Fahlvik, C. Thelander, M. Leijnse, and H. Linke, A quantum-dot heat engine operating close to the thermodynamic efficiency limits, Nat. Nanotechnol. **13**, 920 (2018).

[17] H. Thierschmann, R. Sánchez, B. Sothmann, F. Arnold, C. Heyn, W. Hansen, H. Buhmann, and L. W. Molenkamp, Three-terminal energy harvester with coupled quantum dots, Nat. Nanotechnol. **10**, 854 (2015).

[18] C. Bergenfeldt, P. Samuelsson, B. Sothmann, C. Flindt, and M. Büttiker, Hybrid microwave-cavity heat engine, Phys. Rev. Lett. **112**, 076803 (2014).

[19] R. Sánchez, P. Samuelsson, and P. P. Potts, Autonomous conversion of information to work in quantum dots, Phys. Rev. Res. **1**, 033066 (2019).

[20] K. A. Sablon, J. W. Little, V. Mitin, A. Sergeev, N. Vagidov, and K. Reinhardt, Strong enhancement of solar cell efficiency due to quantum dots with built-in charge, Nano Lett. **11**, 2311 (2011).

[21] G. J. Supran, K. W. Song, G. W. Hwang, R. E. Correa, J. Scherer, E. A. Dauler, Y. Shirasaki, M. G. Bawendi, and V. Bulović, High-performance shortwave-infrared light-emitting devices using core–shell (PbS–CdS) colloidal quantum dots, Adv. Mater. **27**, 1437 (2015).

[22] S. Gustavsson, M. Studer, R. Leturcq, T. Ihn, K. Ensslin, D. C. Driscoll, and A. C. Gossard, Frequency-selective single-photon detection using a double quantum dot, Phys. Rev. Lett. **99**, 206804 (2007).

[23] C. H. Wong and M. G. Vavilov, Quantum efficiency of a single microwave photon detector based on a semiconductor double quantum dot, Phys. Rev. A **95**, 012325 (2017).

[24] W. Khan, P. P. Potts, S. Lehmann, C. Thelander, K. A. Dick, P. Samuelsson, and V. F. Maisi, Efficient and continuous microwave photoconversion in hybrid cavity-semiconductor nanowire double quantum dot diodes, Nat. Commun. **12**, 5130 (2021).

[25] S. Cornia, V. Demontis, V. Zannier, L. Sorba, A. Ghirri, F. Rossella, and M. Affronte, Calibration-free and high-sensitivity microwave detectors based on InAs/InP nanowire double quantum dots, Adv. Funct. Mater. **33**, 2212517 (2023).

[26] A. O. Denisov, S. W. Oh, G. Fuchs, A. R. Mills, P. Chen, C. R. Anderson, M. F. Gyure, A. W. Barnard, and J. R. Petta,

Microwave-frequency scanning gate microscopy of a Si/SiGe double quantum dot, Nano Lett. **22**, 4807 (2022).
[27] Y.-Y. Liu, K. D. Petersson, J. Stehlik, J. M. Taylor, and J. R. Petta, Photon emission from a cavity-coupled double quantum dot, Phys. Rev. Lett. **113**, 036801 (2014).
[28] A. Stockklauser, V. F. Maisi, J. Basset, K. Cujia, C. Reichl, W. Wegscheider, T. Ihn, A. Wallraff, and K. Ensslin, Microwave emission from hybridized states in a semiconductor charge qubit, Phys. Rev. Lett. **115**, 046802 (2015).
[29] M. J. Gullans, Y.-Y. Liu, J. Stehlik, J. R. Petta, and J. M. Taylor, Phonon-assisted gain in a semiconductor double quantum dot maser, Phys. Rev. Lett. **114**, 196802 (2015).
[30] J. Wei, D. Olaya, B. S. Karasik, S. V. Pereverzev, A. V. Sergeev, and M. E. Gershenson, Ultrasensitive hot-electron nanobolometers for terahertz astrophysics, Nat. Nanotechnol. **3**, 496 (2008).
[31] G. Burkard, M. J. Gullans, X. Mi, and J. R. Petta, Superconductor–semiconductor hybrid-circuit quantum electrodynamics, Nat. Rev. Phys. **2**, 129 (2020).
[32] R. Cervantes, G. Carosi, C. Hanretty, S. Kimes, B. H. LaRoque, G. Leum, P. Mohapatra, N. S. Oblath, R. Ottens, Y. Park, G. Rybka, J. Sinnis, and J. Yang, Search for 70 μeV dark photon dark matter with a dielectrically loaded multi-wavelength microwave cavity, Phys. Rev. Lett. **129**, 201301 (2022).
[33] C. R. Valenta and G. D. Durgin, Harvesting wireless power: Survey of energy-harvester conversion efficiency in far-field, wireless power transfer systems, IEEE Microw. Mag. **15**, 108 (2014).
[34] S. Hemour, Y. Zhao, C. H. P. Lorenz, D. Houssameddine, Y. Gui, C.-M. Hu, and K. Wu, Towards low-power high-efficiency rf and microwave energy harvesting, IEEE Trans. Microwave Theory Tech. **62**, 965 (2014).
[35] H. An, S. Ge, W.-Q. Guo, X. Huang, J. Liu, and Z. Lu, Direct detection of dark photon dark matter using radio telescopes, Phys. Rev. Lett. **130**, 181001 (2023).
[36] S. Joshi and G. Moddel, Efficiency limits of rectenna solar cells: Theory of broadband photon-assisted tunneling, Appl. Phys. Lett. **102**, 083901 (2013).
[37] C. Song, Y. Huang, J. Zhou, J. Zhang, S. Yuan, and P. Carter, A high-efficiency broadband rectenna for ambient wireless energy harvesting, IEEE Trans. Antennas Propag. **63**, 3486 (2015).
[38] E. Donchev, J. S. Pang, P. M. Gammon, A. Centeno, F. Xie, P. K. Petrov, J. D. Breeze, M. P. Ryan, D. J. Riley, N. M. Alford *et al.*, The rectenna device: From theory to practice (a review), MRS Energy Sustainability **1**, 1 (2014).
[39] S. Ladan, N. Ghassemi, A. Ghiotto, and K. Wu, Highly efficient compact rectenna for wireless energy harvesting application, IEEE Microw. Mag. **14**, 117 (2013).
[40] L. Namazi, M. Nilsson, S. Lehmann, C. Thelander, and K. A. Dick, Selective GaSb radial growth on crystal phase engineered InAs nanowires, Nanoscale **7**, 10472 (2015).
[41] D. Barker, S. Lehmann, L. Namazi, M. Nilsson, C. Thelander, K. A. Dick, and V. F. Maisi, Individually addressable double quantum dots formed with nanowire polytypes and identified by epitaxial markers, Appl. Phys. Lett. **114**, 183502 (2019).
[42] C. Thelander, P. Caroff, S. Plissard, A. W. Dey, and K. A. Dick, Effects of crystal phase mixing on the electrical properties of InAs nanowires, Nano Lett. **11**, 2424 (2011).
[43] See Supplemental Material at http://link.aps.org/supplemental/10.1103/PhysRevB.109.L081403 for further information on the dc transport measurements, details of our rf heterodyne circuit to measure the photoresponse and internal/external quantum efficiency of the device, theoretical calculations and expressions used in the modeling of the microwave reflectometry and charge transport measurement presented in the main text, and a discussion of the effect of temperature on the power harvesting and photodetection efficiencies, which includes Refs. [46–50].
[44] S. Haldar, H. Havir, W. Khan, S. Lehmann, C. Thelander, K. A. Dick, and V. F. Maisi, Energetics of microwaves probed by double quantum dot absorption, Phys. Rev. Lett. **130**, 087003 (2023).
[45] G. Hackenbroich, B. Rosenow, and H. A. Weidenmüller, Quantum Zeno effect and parametric resonance in mesoscopic physics, Phys. Rev. Lett. **81**, 5896 (1998).
[46] D. Taubert, D. Schuh, W. Wegscheider, and S. Ludwig, Determination of energy scales in few-electron double quantum dots, Rev. Sci. Instrum. **82**, 123905 (2011).
[47] J. Johansson, P. Nation, and F. Nori, Qutip: An open-source Python framework for the dynamics of open quantum systems, Comput. Phys. Commun. **183**, 1760 (2012).
[48] P. P. Potts, A. A. S. Kalaee, and A. Wacker, A thermodynamically consistent Markovian master equation beyond the secular approximation, New J. Phys. **23**, 123013 (2021).
[49] P. Forn-Díaz, L. Lamata, E. Rico, J. Kono, and E. Solano, Ultrastrong coupling regimes of light-matter interaction, Rev. Mod. Phys. **91**, 025005 (2019).
[50] D. Zenelaj, P. P. Potts, and P. Samuelsson, Full counting statistics of the photocurrent through a double quantum dot embedded in a driven microwave resonator, Phys. Rev. B **106**, 205135 (2022).